Biosensors and Bioelectronics 140 (2019) 111358

Contents lists available at ScienceDirect

Biosensors and Bioelectronics

journal homepage: www.elsevier.com/locate/bios

Photoelectrochemical biosensor for CEA detection based on SnS_2-GR with multiple quenching effects of Au@CuS-GR

Di Huang[a], Lu Wang[b], Yi Zhan[a], Lina Zou[a,*], Baoxian Ye[a]

[a] College of Chemistry and Molecular Engineering, Zhengzhou University, Zhengzhou 450001, PR China
[b] School of Environmental Engineering and Chemistry, Luoyang Institute of Science and Technology, Luoyang 471023, PR China

ARTICLE INFO

Keywords:
Photoelectrochemical biosensor
Carcinoembryonic antigen
SnS_2-GR
Au@CuS-GR

ABSTRACT

A novel signal on-off type photoelectrochemical (PEC) biosensing system was designed for sensitive detection of carcinoembryonic antigen (CEA) based on tin disulfide nanosheets loaded on reduced graphene cxide (SnS_2-GR) as the photoactive material and gold nanoparticles coated on reduced graphene oxide-functionalized copper sulfide (Au@CuS-GR) for signal amplification. It's the first time for SnS_2-GR was exploited as a sensing matrix. Here, the photocurrent signals of SnS_2 were amplified attributed to the sensitization effect of graphene. As signal amplifier, Au@CuS-GR could quench the photocurrents of SnS_2-GR not only through the p-n type semiconductor quenching effect as well as the steric hindrance effect, but also as peroxidase mimetics to catalyze the oxidation of 4-Chloro-1-naphthol (4-CN) to produce insoluble product on the electrode surface. Based on the multiple signal amplification ability of Au@CuS-GR, CEA was detected sensitively with a linear range from 0.1 pg mL^{-1} to 10 ng mL^{-1} and limit of detection down to 59.9 fg mL^{-1} (S/N = 3). Meanwhile, the PEC biosensor displayed excellent performance in the assay of human serum sample, showing good application prospects for various target analysis.

1. Introduction

As an emerging and promising technique for biomarkers detection, Photoelectrochemical (PEC) biosensor attracts worldwide attentions, which have distinct advantages of simple operation, fast response and miniaturization (Feng et al., 2018; Qian et al., 2019). Furthermore, due to the separation of the input (light) and output (electricity) signals, the PEC biosensor possesses a low background signal and an excellent sensitivity (Li et al., 2017a; Zeng et al., 2014). Photoactive materials play important role in the performance of PEC biosensors because sensitivity is largely affected by photocurrent changes (Qi et al., 2018). Several typical metal sulfides (e.g. $ZnIn_2S_4$ (Feng et al., 2018), $CuInS_2$ (Wang et al., 2014) and CdS (Zhang et al., 2019)) have been used to constructed PEC biosensors because of their well visible light activities. But the scarcity of indium and the possible environmental impact of Cd^{2+} restricted those biosensors further application (An et al., 2014; Chawla et al., 2017; Huerta Aguilar et al., 2018). Tin disulfide (SnS_2, a typical n-type semiconductor with a visible light band gap of ~2.2 eV) has attracted more research interest in various fields (such as, photocatalysts (An et al., 2014), phototransistors (Zhou et al., 2016) and dye-sensitized solar cells (Cui et al., 2016)) due to its low toxicity, low relative cost and good stability in non-alkaline conditions (Zhang et al., 2017; Liu et al., 2016a). However, the PEC performance of SnS_2 is poor owing to the rapidly recombination of photogenerated electron-hole pairs, which limited its direct application (Wang et al., 2018a). Graphene, as a well-known two-dimensional nanomaterial with the features of large surface area and unique electronic properties, can promote the transfer of electrons in photoactive materials under light irradiation, thus improve the efficiency of the PEC process (Zhang et al., 2014; Zhou et al., 2018). So far, many graphene-based photoactive materials have been utilized to develop high-performance PEC biosensors. For example, based on reduced graphene oxide-functionalized $BiFeO_3$ (GR-$BiFeO_3$), a PEC sensing platform for sensitive, efficient and low cost detection of prostate-specific antigen (PSA) has been described (Zhou et al., 2018). Graphene-doped Bi_2S_3 nanorods have been employed as light photoelectrochemical aptasensing platform for sulfadimethoxine (SDM) detection (Okoth et al., 2016). Therefore, graphene as a conducting scaffold material combined with SnS_2 would be a good choice to improve PEC performances.

Signal amplification method of the signal-off type is an effective strategy to obtain high sensitivity PEC biosensor (Fan et al., 2016). According to the previous literature, the photocurrent change of the signal-off PEC analysis is basically associated with energy transfer (Wang et al., 2017), enzymatic reaction (Zeng et al., 2014; Liu et al.,

* Corresponding author.
E-mail address: zoulina@zzu.edu.cn (L. Zou).

https://doi.org/10.1016/j.bios.2019.111358
Received 27 March 2019; Received in revised form 15 May 2019; Accepted 26 May 2019
Available online 28 May 2019
0956-5663/

2018), steric-hindrance effects (Han et al., 2018; Zhang et al., 2019) and p-n type semiconductor quenching effects (Fan et al., 2016; Yang et al., 2018). Because of p-type semiconductor could compete light energy and electron donor with n-type semiconductor, the quenching effects between p-type and n-type semiconductor was proposed and demonstrated to be very effective (Li et al., 2017b; Wang et al., 2018b). For instance, Wang et al. developed a PEC immunosensor based on CdS sensitized carbon doped titanium dioxide (C–TiO_2/CdS) as photoactive material quenched by SiO_2–CuS composites (Wang et al., 2018b). Fan and co-workers proposed a sandwich-type PEC sensing platform for β-amyloid protein (Aβ) on the basis of ZnO/$Ru(bpy)_3^{2+}$/cerium-doped cadmium sulfide (Ce–CdS) as photoactive matrix and polystyrene@CuS as efficient quencher (Fan et al., 2019). Therefore, the high loading of p-type semiconductor is effective to increase the quenching efficiency. On the other hand, enzymatic catalytic precipitation strategy, which involves the formation of insoluble products on the electrode surface, can affect electron transfer and further improve the detection limits (Chen et al., 2011). Yet, nature enzyme has drawbacks of expensive cost, environmental instability and low catalytic activity easily affected by external conditions, which limited its application in the biosensors (Lan et al., 2016). To overcome these obstacles, various peroxidase-like nanomaterials have been exploited (Chen et al., 2018; Dai et al., 2018). For example, the Histidine-modified Fe_3O_4 (his-Fe_3O_4) nanozyme could acted as peroxidase to induce the generation of the insoluble and insulating precipitation (Li et al., 2019a). A PEC biosensor used silver iodide-chitosan nanoparticle (SICNP) as peroxidase mimetic to catalyze the bioprecipitation reaction was developed (Gong et al., 2016).

Combination of two or more signal amplification ways could effectively enhance the detection sensitivity of PEC biosensor (Dong et al., 2017; Fan et al., 2017; Yang et al., 2018). Copper sulfide (CuS, a typical p-type semiconductor with a direct band gap of 1.2–2.0 eV) loaded on GR as signal labels can achieve higher quenching efficiency. Moreover, CuS-GR exhibit peroxidase-like activity toward peroxidase substrates, which has been proved in the oxidation of 3,3,5,5-tetramethylbenzidine (TMB) to blue product with H_2O_2 (Song et al., 2016). Besides, in order to conjugate these nanomaterials with aptamer, gold nanoparticles (Au NPs) were always to be doped as bonding point, which can conjugate aptamer based on the non-covalent bonding between Au and thiol though bond (Wang et al., 2018c; Zheng et al., 2017; Sun et al., 2016; Yang et al., 2015). Therefore, CuS-GR composited with Au NPs (Au@CuS-GR) would be used as PEC signal amplification probe.

In this work, we proposed a signal on-off type PEC biosensor for highly sensitive detection of CEA based on SnS_2-GR coupled with multiple quenching effects of Au@CuS-GR, as exposed in Scheme 1. Owing to the unique electron transfer ability of GR which effectively enhanced the electron transport on the electrode and thus restrain the recombination of electrons with holes, the photocurrent response of SnS_2-GR was observed to be remarkably promoted than SnS_2 under visible-light irradiation. Upon the sandwich-type specific reaction between aptamers and CEA, Au@CuS-GR bond on the electrode surface specifically to amplify the PEC response signals: (1) the p-type semiconducting CuS from Au@CuS-GR can dramatically weaken the photocurrents of SnS_2-GR because of competitive consumption of electron donors (AA) and light energy of the PEC system (p-n type semiconductor quenching effect); (2) Au@CuS-GR can acts as peroxidase mimics to catalyze the oxidation of 4-Chloro-1-naphthol (4-CN) form insoluble product benzo-4-chloro-1-hexadienone (4-CD) on the electrode surface (mimetic enzymatic catalytic precipitation effect), which resulting in the photocurrent intensity decreased; (3) the steric hindrance effect from the Au@CuS-GR can retard the transport of electron donor, which caused the photocurrents further decreased. Using the Au@CuS-GR to construct PEC biosensors for CEA exhibited good analytical performances.

2. Experiment section

2.1. Materials and reagents

All reagents involved in this work were analytical grade and used as received. Stannic chloride hydrated ($SnCl_4{\cdot}5H_2O$), Copper acetate monohydrate ($CuAc_2{\cdot}H_2O$), thioacetamide (TAA) and Tris (2-carboxyethyl) phosphine hydrochloride (TCEP) were bought from Aladdin Chemistry Co., Ltd., (Shanghai, China). Graphene oxide (GO) was purchased from XianFeng Nano Co. (Nanjing, China). Chloroauric acid ($HAuCl_4{\cdot}3H_2O$) and bovine serum albumin (BSA) were provided by Sigma-Aldrich. Chemical Co. (St. Louis, MO, USA). 4-Chloro-1-naphthol (4-CN) was supplied by Macklin Biochemical Co. Ltd. (Shanghai, China). H_2O_2 (30 wt%) was provided by Tianjin Chemical Reagent Company. Ascorbic acid (AA) was purchased from Sinopharm Chemical Reagent Co., Ltd. (China). 0.1 M Phosphate buffer solution (PBS, pH = 7.4) were derived from the stock solutions of KH_2PO_4, Na_2HPO_4 and KCl, being employed as cleaning solution and detecting bottom liquid which containing 0.1 M AA. Ultrapure water was obtained from a Thermo Scientific Barnstead GenPure water purification system (Shanghai, China). The aptamers squences are obtained from a previous report (Wu et al., 2018; Yang et al., 2017; Zhang et al., 2018). Besides, the aptamers with a thiol on the 5′-end were modified with Au@CuS-GR, and the aptamers with an amino on the 5′- end were immobilized with glutaraldyhyde (GLD). The aptamers for CEA were purchased from Sangon Biotechnology Inc. (Shanghai, China): CEA-aptamers (S1): 5′–NH_2–$(CH_2)_6$-AGG GGG TGA AGG GAT ACC C-3′; CEA-aptamers (S2): 5′–SH–$(CH_2)_6$-ATA CCA GCT TAT TCA ATT-3′. Besides, human serum sample provided by the First Affiliated Hospital of Zhengzhou University (Henan, China) were used as the real sample.

2.2. Apparatus

Transmission electron microscope (TEM, USA FEI, M3000) and Scanning electron microscopy (SEM, JEOL JSM-6700, Japan) could present morphology and structural characterizations of materials. Atomic force microscope (AFM) images were recorded by a Bruker Dimension Icon microscope (USA). X-ray diffractiometer (XRD, Shimadzu, Japan) were recorded with conducted by Cu Ka radiation source (λ = 1.54056 Å). UV–Vis spectra were recorded using a Lambda 35 UV–Vis spectrometer (Beijing, China). All photoelectrochemical measurements were performed on a PEAC200A photochemical reaction apparatus (Tianjin Aida Hengsheng technology development Co.,LTD) equipped with a white 10 W LED lamp. Electrochemical impedance spectroscopy (EIS) and Photocurrent were recorded on RST5000 electrochemical workstation (Zhengzhou Shiruisi Instrument Technology Co. Ltd., China.). A conventional three-electrode system using ITO (4 × 0.5 cm) as working electrode, Pt wire as the auxiliary electrode and saturated Ag/AgCl electrode as the reference electrode was employed.

2.3. Preparation of SnS_2-GR

A one step hydrothermal growth reaction was employed in synthesis of SnS_2-GR. In brief, graphene oxide (GO) (1.36 mg) was dispersed in 7.5 mL ultrapure water with ultrasonic treatment for 4 h to gain a homogeneous suspension. Under constant stirring, $SnCl_4{\cdot}5H_2O$ (262.95 mg) was dissolved in the GO solution. Subsequently, TAA (281.5 mg) was added into above solution, followed by 30min agitation. Then, the obtained mixture solution was sealed into 25 mL Teflon-sealed autoclave and kept at 160 °C for 12 h. The precipitate was collected after centrifuging with ethanol and ultrapure water. The final product dried at 60 °C for 12 h. The preparation of SnS_2 was similar to that of SnS_2-GR without addition of GO.

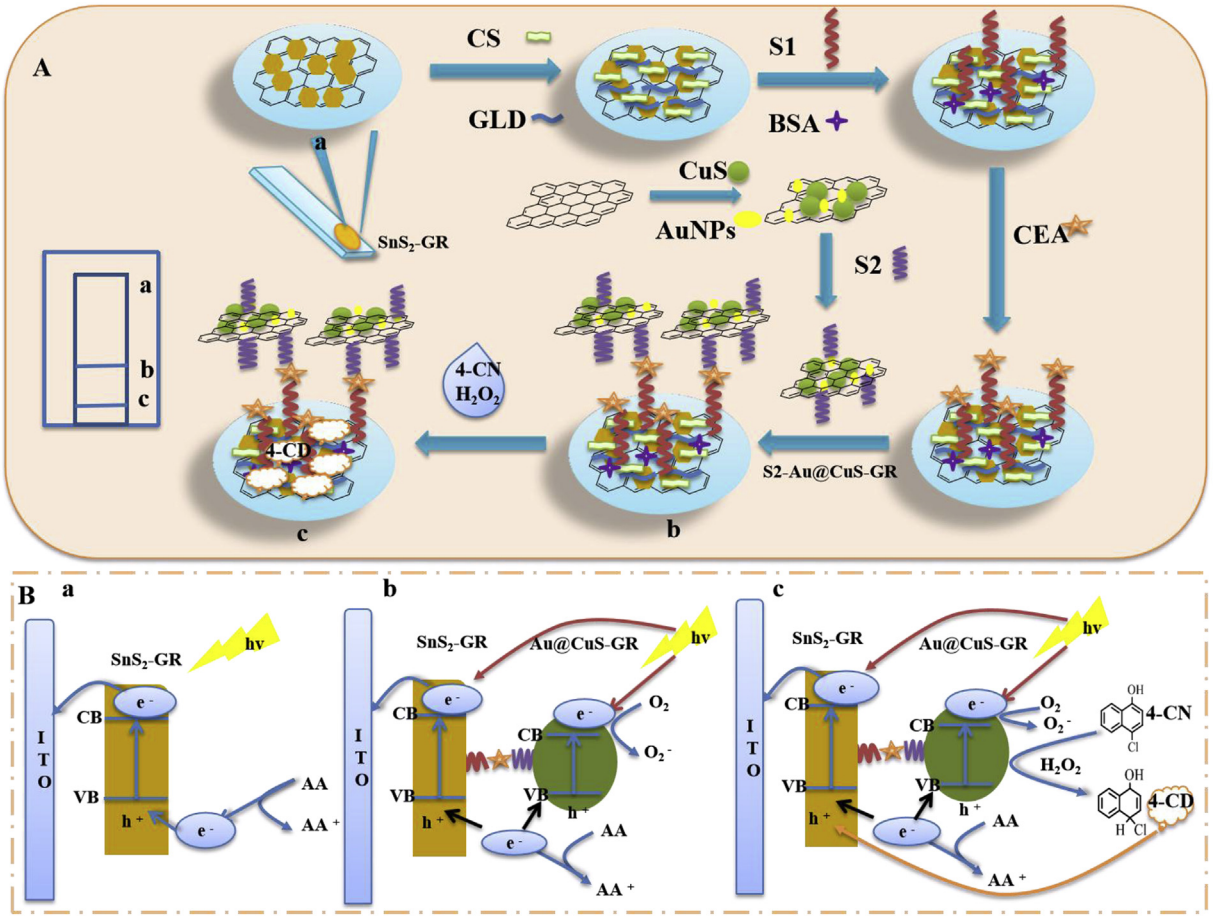

Scheme 1. (A) The PEC biosensor fabrication process and (B) The PEC mechanism in this assay.

2.4. Preparation of S2–Au@CuS-GR

Au@CuS-GR was prepared according to the improved synthetic method (Song et al., 2016). The details were described in Supplementary Material.

S2 was conjugated with Au@CuS-GR through the bond of Au–S (Wang et al., 2018c; Zheng et al., 2017; Sun et al., 2016). To reduce the disulfide bond of S2, 10 μL 20 μM S2 was mixed with 10 μL 2 mM TCEP for 1.5 h at room temperature (Liu et al., 2016b). Then above solution was added into 500 μL Au@CuS-GR solution and incubated for 12 h at 4 °C. After the mixed product was centrifuged under 10000 rpm for 5 min to remove unbound S2, the sediment was dispersed in 500 μL 0.1 M PBS (pH = 7.4) containing 1% BSA and further incubated for 1 h to eliminate nonspecific binding sites. After twice centrifuging to remove excess BSA, the S2–Au@CuS-GR was redispersed in 500 μL 0.1 M PBS (pH = 7.4) for further experiment.

2.5. Construction of the PEC biosensor and PEC measurement

Prior to modification, ITO electrodes were washed successively by acetone, ethanol and ultrapure water with ultrasonic and dried with N_2 for following using. First of all, 10 μL 3 mg/mL SnS_2-GR water dispersion was spread onto the surface of ITO electrode and dried under the infrared lamp. Subsequently, 10 μL 1% acetic acid containing 0.1 wt% chitosan (CS) was covered onto the ITO/SnS_2-GR electrode surface. After dried at 60 °C, 10 μL 2.5% glutaraldyhyde (GLD) was deposited on the electrode surface and maintained for 1 h at room temperature. After thoroughly washing with ultrapure water, the unbound and physically adsorbed GLD were removed. Next, 10 μL 4 μM S1 was dropped on the above electrode for 40 min at 37 °C. After washing with 0.1 M PBS (pH = 7.4) to remove unbound S1, 10 μL 1 wt% BSA was covered on the obtained electrode for 1 h to block residual sites. After that, 10 μL different concentrations of CEA were casted on above electrode for 40 min at 37 °C. Then the electrode was incubated with 10 μL of S2–Au@CuS-GR for 1 h at 37 °C and washed with 0.1 M PBS (pH = 7.4). Finally, to finishing the mimetic enzymatic catalytic precipitation (MECP) reaction, the obtained electrode (ITO/SnS_2-GR/CS/S1/BSA/CEA/S2–Au@CuS-GR) was incubated with 1 mM H_2O_2 solution containing 1 mM 4-CN for 20 min at room temperature. And then the finally electrode was washed by ultrapure water. All of PEC measurements were performed at 0.1 M PBS (pH = 7.4) containing 0.1 M AA at 0.2 V.

3. Results and discussion

3.1. Characterization of the SnS_2-GR

The morphologies of the GO and SnS_2-GR were characterized by SEM and TEM. Compared with pure GO (Fig. 1A) and pure SnS_2 (Fig. 1B, D), Fig. 1C image shown that small-sized SnS_2 nanosheets was deposited on GR. The TEM image in Fig. 1E revealed that SnS_2 nanosheets were uniformly decorated on GR sheets without aggregation. The X-ray diffraction (XRD) patterns of the GO, GR, SnS_2 and SnS_2-GR were recorded in Fig. 2. As shown in curve a, GO presented a single diffraction peak at around 12.5° corresponding to (001). After GO was successfully reduced, the diffraction peak shift from 12.5° to 24° (curve b) (Duan et al., 2018). Besides, it can be seen that the diffraction peaks of SnS_2-GR (curve d) at about 15, 28.2, 32.1, 42.0, 50.0 and 52.5° are matched well with the diffraction peaks of (002), (100), (112), (104), (110) and (004) planes of hexagonal SnS_2 (JCPDS 23–0677) (curve c)

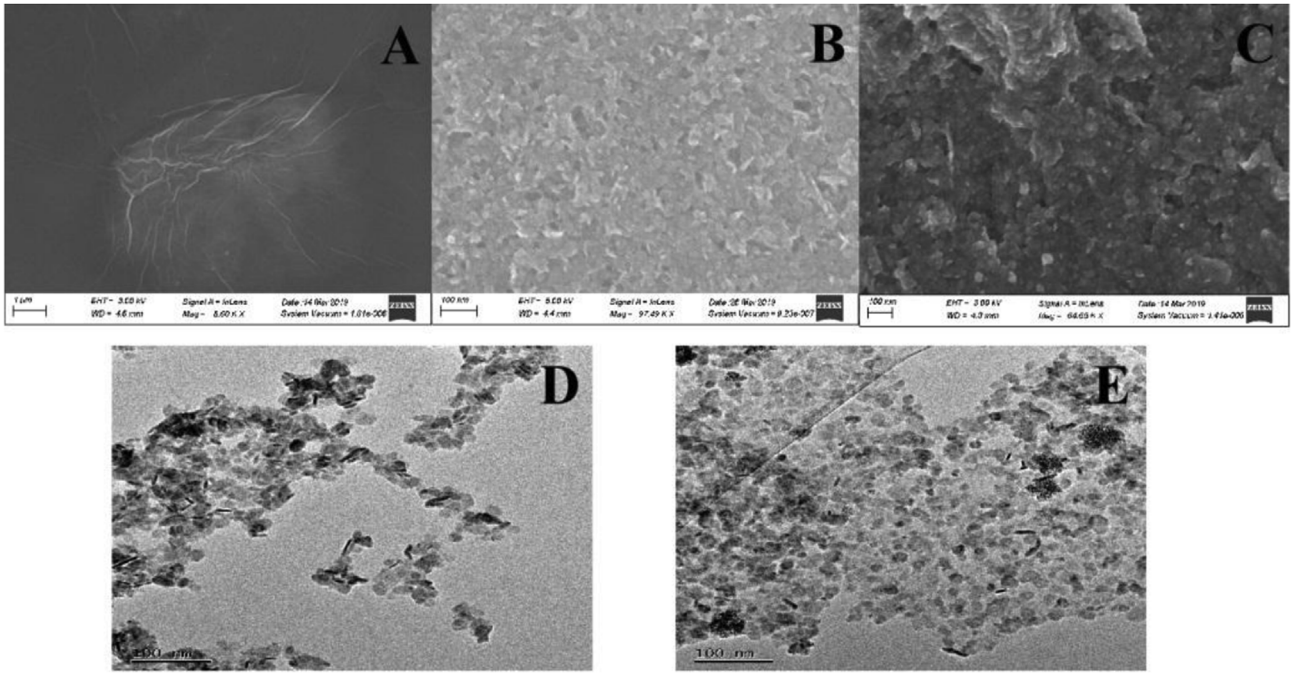

Fig. 1. SEM images of GO (A), SnS_2 (B) and SnS_2-GR (C). TEM images of SnS_2 (D) and SnS_2-GR (E).

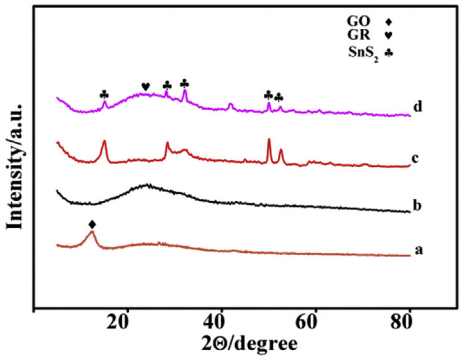

Fig. 2. XRD patterns of the GO (a), GR (b), SnS_2 (c) and SnS_2-GR (d).

(An et al., 2014). The above mentioned results confirmed the successful synthesis of SnS_2-GR.

In order to confirm the promising application of SnS_2-GR in PEC biosensor and the benefit of GR for electron transfer during the PEC process, electrochemical impedance spectroscopy (EIS) and PEC method were employed. In this assay, EIS measurements were carried out in 5×10^{-3} M $[Fe(CN)_6]^{3-/4-}$ containing 1×10^{-1} M KCl. Each impedance spectrum has two parts (a partial semicircle and a linear profile) (Li et al., 2018). The semicircle diameter equals the charge transfer resistance (R_{ct}) (Fu et al., 2017). As displayed in Fig. 3A, the R_{ct} of ITO/SnS_2 electrode (curve b) was obviously larger than that of ITO electrode (curve a) for the weak conductivity of semiconductors. However, the smallest R_{ct} of ITO/SnS_2-GR electrode (curve c) indicated that GR can accelerate charge transfer remarkably in this study. As show in Fig. 3B, there was no photocurrent on the bare ITO electrode (curve a). Besides, the photocurrent of ITO/SnS_2-GR electrode (curve c) exhibited much higher than that of ITO/SnS_2 electrode (curve b), revealing that the incorporation of graphene could enhance the electron transport and restrain the recombination of electrons with holes. Thus, based on above experiment results, SnS_2-GR as a new photoactive material used to construct PEC biosensor.

3.2. Characterization of the Au@CuS-GR

The successful synthesis of CuS-GR and Au@CuS-GR were visually observed by SEM and TEM. As shown in the inset of Fig. S1A and Fig. S1B, the CuS NPs decorated on GR without aggregation. Besides, from the SEM image in Fig. S1A and the TEM images of Au@CuS-GR in Fig. S1C, the Au NPs and CuS NPs appear to be distributed on the surface of GR. The element analysis of Au@CuS-GR was confirmed through XRD (Fig. S1D). The diffraction peaks of CuS-GR (curve d) were similar with that of CuS (JCPDS 06–0464) (curve b) (Qin et al., 2012), showing that the CuS had good crystallinity on GR. After in-suit reduction of Au NPs on CuS-GR, almost every diffraction peak of GR-Au NPs (curve b) and CuS-GR (curve d) can be seen in Au@CuS-GR (curve e), which suggested the formation of Au NPs on the CuS-GR and their crystalline nature.

In addition, the peroxidase-like activities of Au@CuS-GR was directly tested in TMB-H_2O_2 reaction system (Wu et al., 2018). As shown in Fig. S2, TMB + H_2O_2 system (tube a, curve a) was colorless. After the Au@CuS-GR was added, the mixture turned blue and new absorption peaks at 453 and 653 nm appeared (tube d, curve d). Correspondingly, in the case of H_2O_2 absent, Au@CuS-GR + TMB system (tube b, curve b) has no peaks at 453 and 653 nm. These results indicated that Au@CuS-GR have peroxidase-like properties.

3.3. EIS and PEC characterization of the developed PEC biosensor

The interfacial resistance changes during the construction process were investigated by EIS. As shown in Fig. 4A, the ITO/SnS_2-GR electrode showed the smallest R_{ct} (curve a). After CS, S1 and BSA was coated on ITO/SnS_2-GR electrode step by step, the R_{ct} increased in sequence (curve b ~ d). This phenomenon can be attributed to weak conductivity of CS and single strand-DNA and insulating property of protein. With CEA and S2–Au@CuS-GR were incubated on PEC biosensor in order, the R_{ct} continuously increased (curve e, f), which reflected that the process of binding two aptamers to the same CEA molecule to form a sandwich complex (S1-CEA-S2) (Xue et al., 2015; Shu et al., 2013) was successful completed. And S2–Au@CuS-GR was successful bond on the electrode. Additionally, after the obtained PEC biosensor completed MECP reaction, the R_{ct} further enlarged (curve g).

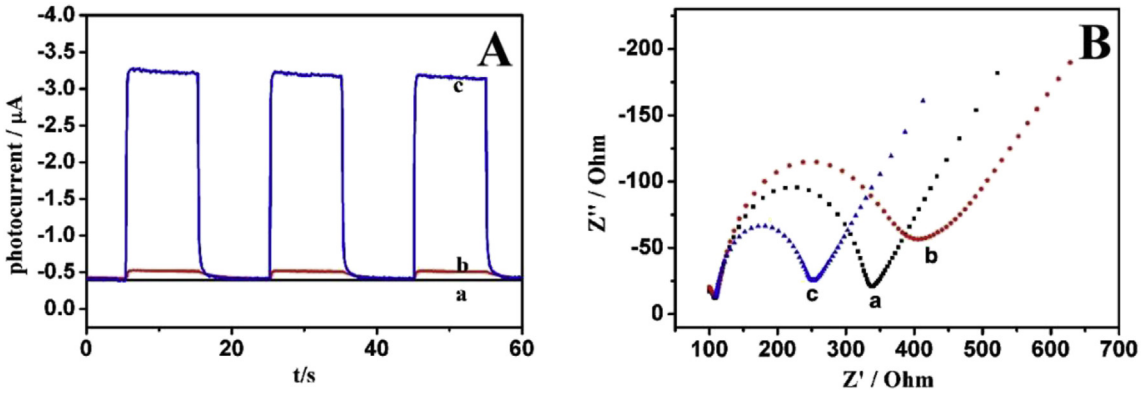

Fig. 3. (A) EIS Nyquist plots and (B) time-based photocurrent response curves of ITO (a), ITO/SnS_2 (b) and ITO/SnS_2-GR (c).

The reason is that in the presence of H_2O_2, Au@CuS-GR exhibited good peroxidase-like property to catalyze 4-CN oxidation and generate insoluble 4-CD deposits on the electrode, which can hinder electron transfer. The EIS results revealed the successful construction of PEC biosensor.

The stepwise assembly process of the PEC biosensor and the interface properties of electrodes was also be evaluated by PEC method. As shown in Fig. 4B, the ITO/SnS_2-GR electrode showed the highest photocurrent (curve a). Subsequently, the photocurrent gradually decreased with immobilization of CS, S1, BSA and CEA specific binding on the ITO/SnS_2-GR electrode step by step (curve b ~ e). This was because linker moleculars and biomoleculars hindered electron donors (AA) to the electrode surface (poor charge-transfer and steric hindrance). In addition, when S2–Au@CuS-GR was bond to the above electrode, the photocurrent decreased (curve f), which owing to the large steric hindrance and p-n type semiconductor quenching effect of the S2–Au@CuS-GR. At last, after the above electrode was incubated with 1 mM H_2O_2 solution containing 1 mM 4-CN for 20 min at room temperature, the photocurrent intensity further decreased (curve g). Because that the insoluble oxidation product 4-CD was generated on the electrode surface by the catalysis of Au@CuS-GR. Both the EIS and PEC results confirmed that a highly sensitive PEC biosensor based on Au@CuS-GR was successfully constructed. In addition, atomic force microscopy (AFM) was used to further verification of the successful fabrication of the PEC biosensor. More detailed information can be seen in the Supplementary Material (Fig. S3).

To further investigate the feasibility of the amplified strategy, S2-GR-AuNPs and S2–Au@CuS-GR were applied to constructed PEC biosensors for target CEA (1 ng mL^{-1}). As shown in Fig. S4, when the PEC biosensor was immobilized with S2-GR-AuNPs (cure a), the photocurrent is higher than that of immobilized with S2–Au@CuS-GR (cure c), which indicating CuS NPs could weaken the photocurrents of SnS_2-GR though p-n type semiconductor quenching effect. After treating in 20 min in 1 mM H_2O_2 solution containing 1 mM 4-CN, the photocurrent of PEC biosensor labeling with S2–Au@CuS-GR (cure d) caused higher photocurrent change than that of labeling with S2-GR-AuNPs (cure b), suggesting the insoluble precipitation (4-CD) was generated on the electrode surface.

3.4. Optimization of experimental conditions

In order to achieve the excellent sensitivity of the PEC biosensor for CEA assay, various experiment conditions were optimized, including the applied potential, the concentration of S1, incubation time of target CEA and catalytic deposition time of 4-CN.

Fig. S5A showed the effect of the applied potential in the ITO/SnS_2-GR electrode, which was a key parameter for producing the photocurrent. With increasing of potential, the photocurrent improved remarkably from 0 to 0.2 V and then reached a platform after 0.2 V, which indicated high applied potential was beneficial for restraining the recombination rate of the electron-hole pairs in this work. The interference species in the sample could eliminate in low applied potential detection. Accordingly, 0.2 V was selected as the optimum applied potential for PEC detection.

Fig. S5B showed the effect of S1 concentration. Due to the poor conductivity of single strand DNA, the photocurrent decreased along with S1 concentration increased from 1 to 5 μM. Besides, the photocurrent nearly reached a platform at 4 μM, suggesting the saturated immobilization of S1 on ITO/SnS_2-GR/CS electrode. Therefore, the optimum concentration of S1 was 4 μM.

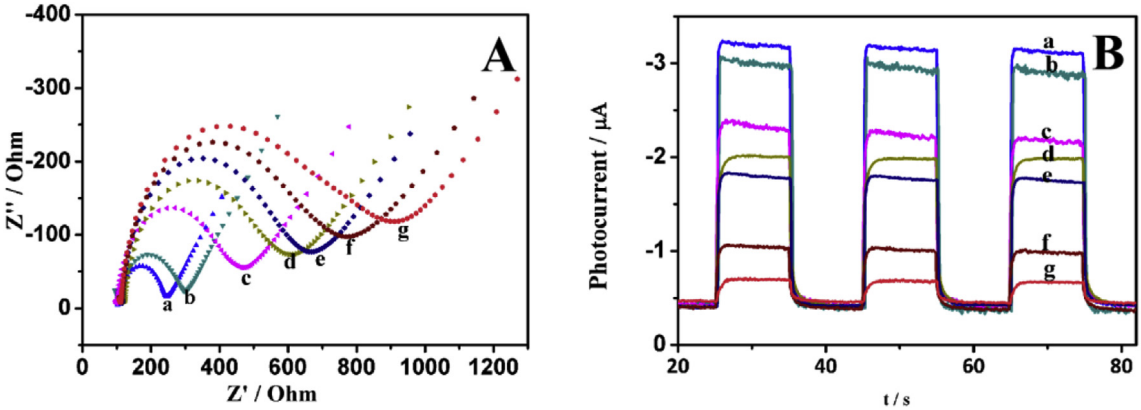

Fig. 4. (A) EIS Nyquist plots and (B) time-based photocurrent response curves of ITO/SnS_2-GR (a), ITO/SnS_2-GR/CS (b), ITO/SnS_2-GR/CS/S1 (c), ITO/SnS_2-GR/CS/S1/BSA (d), ITO/SnS_2-GR/CS/S1/BSA/CEA (e), ITO/SnS_2GR/CS/S1/BSA/CEA/S2–Au@CuS-GR (f) and ITO/SnS_2-GR/CS/S1/BSA/CEA/S2–Au@CuS-GR after incubation with 1 mM 4-CN and 1 mM H_2O_2 for 20 min (g).

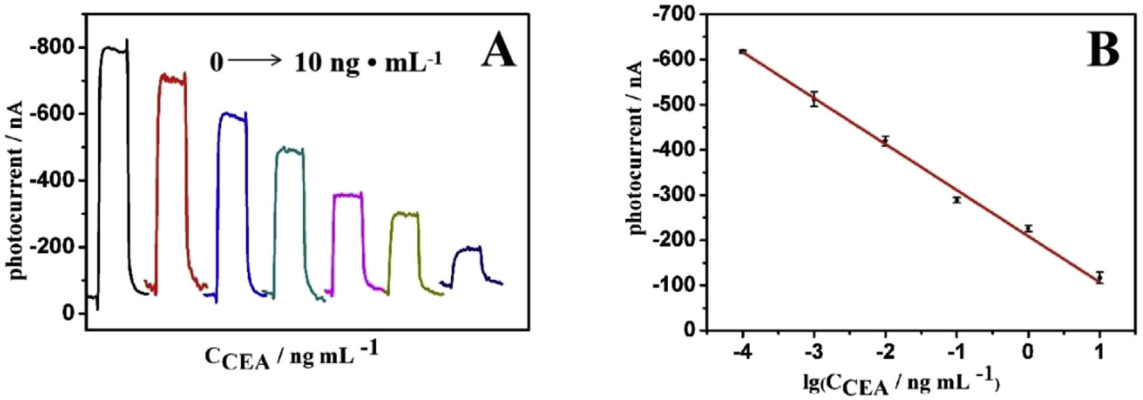

Fig. 5. (A) PEC responses of the biosensor to 0, 0.0001, 0.001, 0.01, 0.1, 1 and 10 ng mL^{-1} CEA. (B) Linear calibration curve.

Fig. S5C exhibited the effect of incubation time of target CEA (1 ng mL^{-1}). With increasing incubation time, the photocurrent decreased and tend to stable, forecasting the completely reaction between S1 and CEA in 40 min. Consequently, 40 min was accepted as the optimal incubation time for PEC sensing.

Fig. S5D depicted the effect of MECP time on the photocurrents of PEC biosensor. Because of the longer MECP time generating more insoluble 4-CD on the electrode surface, the photocurrent decreased alone with MECP time extending, then it reaches a plateau after 20 min when MECP reaction was complete. Thus, 20 min was taken as the optimal MECP time.

3.5. PEC biosensor for CEA

Under the experimental conditions optimized above, the novel PEC biosensor with SnS_2-GR modified ITO electrode and signal amplification of Au@CuS-rGO was applied for the determination of CEA. From Fig. 5A, due to Au@CuS-GR provide a signal-off strategy, the decreased photocurrent is directly related to the increased concentration of CEA (0–10 ng mL^{-1}). Fig. 5B showed that the logarithm of CEA concentration was linear with the photocurrent in the range from 0.1 pg mL^{-1} to 10 ng mL^{-1}. The regression equation is I (nA) = 0.1019 lg C (ng mL^{-1}) - 0.2089 with the correlation coefficient was 0.9952. Furthermore, the detection limit was estimated to be 59.9 fg mL^{-1} (S/N = 3), which was more lower than other methods for CEA detection (Table 1).

3.6. Specificity, repeatability and stability of the PEC biosensor

In order to assess the specificity of the proposed sensing method for CEA, several interfering species, including thrombin (TB), hemoglobin (Hb), prostate specific antigen (PSA) and L-cysteine (L-cys) were investigated. As illustrated in Fig. 6A, even if the above interfering species were 10-fold larger than CEA (1 ng mL^{-1}), the photocurrent of interfering species were similar as that of blank sample. In contrast, in the presence of target CEA (1 ng mL^{-1}), photocurrent was significantly different from that of blank sample, which was obviously lower. Above results indicated the high specificity of the PEC biosensor for CEA.

The reproducibility of the PEC biosensor was measured with three parallel sensors. The relative standard deviations were 1.60%, 1.07% and 0.61% towards 0.001, 0.01, and 0.1 ng mL^{-1} of CEA. The results suggested the acceptable reproducibility of this biosensor. Additionally, the stability was another vital factor to be investigated. As shown in Fig. 6B, after 8 on/off irradiation cycles, the photocurrents were stable without noticeable change, indicating the stable response for signal collection.

3.7. Real sample analysis

To investigate the applicability and reliability of the PEC biosensor, the detection of CEA in human serum sample were performed. Prior to assay, the human serum sample was diluted to 10-fold with 0.1 M PBS (pH = 7.4) to avoid the level of CEA in the human serum sample were over the calibration range. The results were show in Table S1. Compared with the human serum sample were determined by the commercial CEA ELISA kit (note: The assays by using commercial CEA ELISA kit purchased from Zhengzhou Biocell antibody center (Zhengzhou, China) toward these samples were finished by the hospital), the relative deviations between the two methods were less than 6.9%, indicating the practical applications of this method to detect CEA.

4. Conclusion

In summary, benefiting from combined multiple quenching effects of Au@CuS-GR and SnS_2-GR, a novel signal on-off type PEC biosensor for highly sensitive detection of CEA was constructed. For signal on, the photocurrent of ITO/SnS_2-GR was much higher than that of ITO/SnS_2 because graphene could promote the electron transfer in photoactive

Table 1
Analytical performances of different methods for CEA detection.

Method	detection range (ng/mL)	detection limit (pg/mL)	references
Voltammetric enzyme-linked immunosorbent assay (ELISA)	0.50–80	500	Zhang et al. (2008)
Endonuclease-linked multiplex immunoassay	0.001–10	0.3	Gan et al. (2018)
ELISA	0.1–20	350	Li et al. (2019b)
	5–20	1100	
Electrochemical aptasensor	0.005–50	1.5	Wen et al. (2016)
Colorimetric aptasensor	0.1–8	60	Zou and Wang, 2017
electrochemiluminescence aptasensor	0.0008–4	0.28	Yang et al. (2017)
Amperometric aptasensor	1–5000	1.2	Paniagua et al. (2019)
Photoelectrochemical aptasensor	0.005–5	1.9	Qiu et al. (2018)
Photoelectrochemical aptasensor	0.001–500	4.8	Qiu et al. (2019)
Photoelectrochemical aptasensor	0.0001–10	0.0599	This work

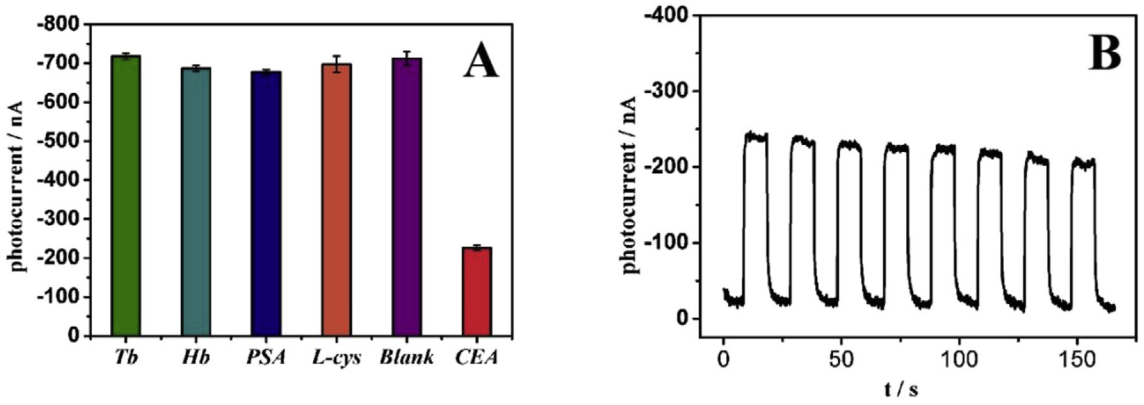

Fig. 6. (A) Specificity of the PEC biosensor toward CEA (1 ng mL $^{-1}$) and other interferents (10 ng mL^{-1}). (B) The stability of the PEC biosensor under 8 on/off irradiation cycles.

materials. For signal off, due to several inhibition effect (p-n type semiconductor quenching effect, mimetic enzymatic catalytic precipitation effect and the steric hindrance effect), the Au@CuS-GR could efficiently weaken the photocurrent of the SnS_2-GR. Finally, this developed PEC biosensor presented high selectivity and sensitivity, which was successfully used for human serum sample detection. However, the developed PEC biosensor needs about 7 h to complete the multiple layer of modification, which limited its further application. Therefore, to develop washing free and automatic detection strategy for the target is our effort in the future.

Declaration of interests

The authors declare that they have no known competing financial interests or personal relationships that could have appeared to influence the work reported in this paper.

CRediT authorship contribution statement

Di Huang: Conceptualization, Methodology, Validation, Formal analysis, Investigation, Resources, Data curation, Writing - original draft, Writing - review & editing. **Lu Wang:** Validation, Formal analysis, Methodology, Investigation. **Yi Zhan:** Formal analysis, Methodology, Investigation. **Lina Zou:** Data curation, Writing - review & editing, Project administration. **Baoxian Ye:** Formal analysis, Methodology, Investigation.

Acknowledgements

This work was supported by the National Natural Science Foundation of China (Grant no. U1504216; 21575130) and Startup Research Fund of Zhengzhou University (Grant no. 1511316006).

Appendix A. Supplementary data

Supplementary data to this article can be found online at https://doi.org/10.1016/j.bios.2019.111358.

References

An, X., Yu, J.C., Tang, J., 2014. J. Mater. Chem. A. 2, 1000.
Chawla, R., Singhal, P., Garg, A.K., 2017. J. Inf. Technol. 10, 265–277.
Chen, H.Y., Xu, J.J., Dong, X.Y., Yu, P.P., Ma, Z.Y., Zhao, W.W., 2011. Anal. Chem. 84, 917–923.
Chen, J., Chen, S., Qin, Z., Li, C.R., Xu, W., Qiu, J.F., 2018. Microchim. Acta. 185, 2–9.
Cui, X., Xu, W., Xie, Z., Wang, Y., 2016. J. Mater. Chem. A. 4, 1908–1914.
Dai, H., Chen, Y., Niu, X., Pan, C., Chen, H.L., Chen, X., 2018. Biosens. Bioelectron. 118, 36–43.
Dong, Y., Cao, J., Liu, Y., Ma, S., 2017. Biosens. Bioelectron. 91, 246–252.
Duan, Y., Li, S., Lei, S., Qiao, J., Zou, L., Ye, B., 2018. J. Electroanal. Chem. 827, 137–144.
Fan, G.C., Zhu, H., Du, D., Zhang, J.R., Zhu, J.J., Lin, Y., 2016. Anal. Chem. 88, 3392–3399.
Fan, D., Ren, X., Wang, H., Wu, D., Zhao, D., Chen, Y., Wei, Q., Du, B., 2017. Biosens. Bioelectron. 87, 593–599.
Fan, D., Liu, X., Bao, C., Feng, J., Wang, H., Ma, H., Wu, D., Wei, Q., 2019. Biosens. Bioelectron. 129, 124–131.
Feng, J., Li, F., Li, X., Wang, Y., Fan, D., Du, B., Li, Y., Wei, Q., 2018. Biosens. Bioelectron. 117, 773–780.
Fu, Y., Wang, L., Huang, D., Zou, L., Ye, B., 2017. J. Electroanal. Chem. 801, 77–83.
Gan, N., Xie, L., Zhang, K., Cao, Y., Hu, F., Li, T., 2018. Sensor. Actuator. B. 272, 526–533.
Gong, L., Dai, H., Zhang, S., Lin, Y., 2016. Anal. Chem. 88, 5775–5782.
Han, Q., Wang, R., Xing, B., Zhang, T., Khan, M.S., Wu, D., Wei, Q., 2018. Biosens. Bioelectron. 99, 493–499.
Huerta Aguilar, C.A., Narayanan, J., Shanmuganathan, R., Ricardo, C.T., Avilés Castrillo, J.I., Piña Miranda, M.Y., Aguilar Pérez, K.M., 2018. J. Photochem. Photobiol. A Chem. 367, 1–12.
Lan, F., Sun, G., Liang, L., Ge, S., Yan, M., Yu, J., 2016. Biosens. Bioelectron. 79, 416–422.
Li, M., Tang, D., Lin, Z., Zhang, K., Lv, S., 2017a. Biosens. Bioelectron. 101, 159–166.
Li, M.J., Zheng, Y.N., Liang, W. Bin, Yuan, R., Chai, Y.Q., 2017b. ACS Appl. Mater. Interfaces 9, 42111–42120.
Li, S., Duan, Y., Lei, S., Qiao, J., Li, G., Ye, B., 2018. Sensor. Actuator. B. 274, 218–227.
Li, W., Fan, G.C., Gao, F., Cui, Y., Wang, W., Luo, X., 2019a. Biosens. Bioelectron. 127, 64–71.
Li, N., Yue, X., Zhang, L., Wang, K., Zhang, J., Zhang, Z., Dang, F., 2019b. J. Mater. Chem. B. 2242–2246.
Liu, Y., Zhang, Y., Wu, D., Fan, D., Pang, X., Zhang, Y., Ma, H., 2016a. Biosens. Bioelectron. 86, 301–307.
Liu, Q., Huan, J., Dong, X., Qian, J., Hao, N., You, T., Mao, H., Wang, K., 2016b. Sensor. Actuator. B 235, 647–654.
Liu, L., Fan, G., Zhang, J., Zhu, J., 2018. Anal. Chim. Acta 1027, 33–40.
Okoth, O.K., Yan, K., Liu, Y., Zhang, J., 2016. Biosens. Bioelectron. 86, 636–642.
Paniagua, G., Villalonga, A., Eguílaz, M., Vegas, B., Parrado, C., Rivas, G., Díez, P., Villalonga, R., 2019. Anal. Chim. Acta 1061, 84–91.
Qi, Z., Li, L., Wong, D.K.Y., Tang, Y., Liu, P., Liu, X., Li, D., Yang, L., 2018. Biosens. Bioelectron. 112, 193–201.
Qian, Y., Feng, J., Fan, D., Zhang, Y., Kuang, X., Wang, H., Wei, Q., Ju, H., 2019. Biosens. Bioelectron. 131, 299–306.
Qin, X., Zhang, Y., Al Youbi, A.O., Tian, J., Li, H., Asiri, A.M., Wang, L., Sun, X., 2012. Langmuir 28, 12893–12900.
Qiu, Z., Shu, J., Tang, D., 2018. Anal. Chem. 90, 12214–12220.
Qiu, Z., Shu, J., Liu, J., Tang, D., 2019. Anal. Chem. 91, 1260–1268.
Shu, H.W., Wen, W., Xiong, H.Y., Zhang, X.H., Wang, S.F., 2013. Electrochem. Commun. 37, 15–19.
Song, W., Nie, G., Ji, W., Jiang, Y., Lu, X., Zhao, B., Ozaki, Y., 2016. RSC Adv. 6, 54456–54462.
Sun, D., Lu, J., Zhong, Y., Yu, Y., Wang, Y., Zhang, B., Chen, Z., 2016. Biosens. Bioelectron. 75, 301–307.
Wang, S., Zhu, Y., Yang, X., Li, C., 2014. Electroanalysis 26, 573–580.
Wang, B., Dong, Y.X., Wang, Y.L., Cao, J.T., Ma, S.H., Liu, Y.M., 2017. Sensor. Actuator. B 254, 159–165.
Wang, Y., Fan, D., Zhao, G., Feng, J., Wei, D., Zhang, N., Cao, W., 2018a. Biosens. Bioelectron. 120, 1–7.
Wang, X., Gao, P., Yan, T., Li, R., Xu, R., Zhang, Y., Du, B., Wei, Q., 2018b. Sensor. Actuator. B. 258, 1–9.
Wang, Y.H., Xia, H., Huang, K.J., Wu, X., Ma, Y.Y., Deng, R., Lu, Y.F., Han, Z.W., 2018c. Microchim. Acta 185, 1–7.
Wen, W., Huang, J.Y., Bao, T., Zhou, J., Xia, H.X., Zhang, X.H., Wang, S.F., Zhao, Y. Di, 2016. Biosens. Bioelectron. 83, 142–148.
Wu, Y., Li, G., Zou, L., Lei, S., Yu, Q., Ye, B., 2018. Sensor. Actuator. B 259, 372–379.
Xue, S., Yi, H., Jing, P., Xu, W., 2015. RSC Adv. 5 (94), 77454–77459.
Yang, Z.H., Zhuo, Y., Yuan, R., Chai, Y.Q., 2015. ACS Appl. Mater. Interfaces 7, 10308–10315.

Yang, J.J., Cao, J.T., Wang, Y.L., Wang, H., Liu, Y.M., Ma, S.H., 2017. J. Electroanal. Chem. 787, 88–94.
Yang, R., Zou, K., Li, Y., Meng, L., Zhang, X., Chen, J., 2018. Anal. Chem. 90, 9480–9486.
Zeng, X., Bao, J., Han, M., Tu, W., Dai, Z., 2014. Biosens. Bioelectron. 54, 331–338.
Zhang, S., Yang, J., Lin, J., 2008. Bioelectrochemistry 72 (1), 47–52.
Zhang, X., Xu, F., Zhao, B., Ji, X., Yao, Y., Wu, D., 2014. Electrochim. Acta 133, 615–622.
Zhang, Y., Liu, Y., Li, R., Khan, M.S., Gao, P., Zhang, Y., 2017. Sci. Rep. 7, 4629.
Zhang, X., Bao, N., Luo, X., Ding, S.N., 2018. Biosens. Bioelectron. 114, 44–51.
Zhang, B., Wang, H., Zhao, F., Zeng, B., 2019. Electrochim. Acta 297, 372–380.
Zheng, J., Zhang, M., Guo, X., Wang, J., Xu, J., 2017. Sensor. Actuator. B. 250, 8–16.
Zhou, X., Zhang, Q., Gan, L., Li, H., Zhai, T., 2016. Adv. Funct. Mater. 26, 4405–4413.
Zhou, Q., Lin, Y., Zhang, K., Li, M., Tang, D., 2018. Biosens. Bioelectron. 101, 146–152.
Zou, M., Wang, S., 2017. Korean Chem. Soc. 38, 1143–1148.